ACS Catalysis

Research Article

pubs.acs.org/acscatalysis

Probing Ultrathin One-Dimensional Pd−Ni Nanostructures As Oxygen Reduction Reaction Catalysts

Haiqing Liu,[†] Christopher Koenigsmann,[†] Radoslav R. Adzic,[‡] and Stanislaus S. Wong*[,†,§]

[†]Department of Chemistry, State University of New York at Stony Brook, Stony Brook, New York 11794-3400, United States

[‡]Chemistry Department, Brookhaven National Laboratory, Building 555, Upton, New York 11973, United States

[§]Condensed Matter Physics and Materials Sciences Department, Brookhaven National Laboratory, Building 480, Upton, New York 11973, United States

Supporting Information

ABSTRACT: An ambient, surfactant-based synthetic means was used to prepare ultrathin binary ($d \sim 2$ nm) Pd−Ni nanowires, which were subsequently purified using a novel butylamine-based surfactant-exchange process coupled with an electrochemical CO adsorption and stripping treatment to expose active surface sites. We were able to systematically vary the chemical composition of as-prepared Pd−Ni nanowires from pure elemental Pd to $Pd_{0.50}Ni_{0.50}$ (atomic ratio), as verified using EDS analysis. The overall morphology of samples possessing >60 atom % Pd consisted of individual, discrete one-dimensional nanowires. The electrocatalytic performances of elemental Pd, $Pd_{0.90}Ni_{0.10}$, $Pd_{0.83}Ni_{0.17}$, and $Pd_{0.75}Ni_{0.25}$ nanowires in particular were examined. Our results highlight a "volcano"-type relationship between chemical composition and corresponding ORR activities with $Pd_{0.90}Ni_{0.10}$, yielding the highest activity (i.e., 1.96 mA/cm^2 at 0.8 V) among all nanowires tested. Moreover, the $Pd_{0.90}Ni_{0.10}$ sample exhibited outstanding methanol tolerance ability. In essence, there was only a relatively minimal 15% loss in the specific activity in the presence of 4 mM methanol, which was significantly better than analogous data on Pt nanoparticles and Pt nanowires. In addition, we also studied ultrathin, core−shell Pt∼$Pd_{0.90}Ni_{0.10}$ nanowires, which exhibited a specific activity of 0.62 mA/cm^2 and a corresponding mass activity of 1.44 A/mg_{Pt} at 0.9 V. Moreover, our as-prepared core−shell electrocatalysts maintained excellent electrochemical durability. We postulate that one-dimensional Pd−Ni nanostructures represent a particularly promising platform for designing ORR catalysts with high performance.

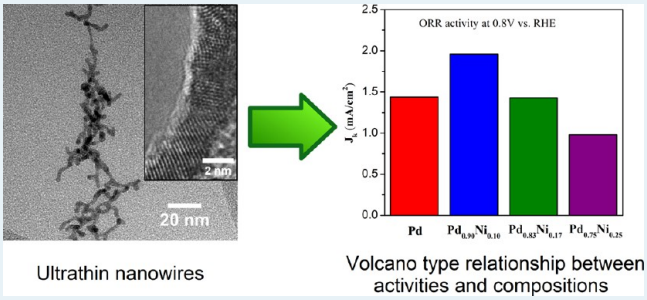

KEYWORDS: *Pd−Ni, binary electrocatalyst, ORR, methanol tolerance, core−shell structure*

1. INTRODUCTION

A growing demand for efficient, low-cost, renewable energy has sparked a good deal of interest in the commercial development of fuel cell technology as a replacement for combustion-based energy sources. Direct methanol fuel cell (DMFC) technology represents a potential fuel cell option for future applications in the automotive,[1] portable power,[2,3] and electronics industries.[4] Specifically, DMFCs, which utilize methanol as a renewable fuel source, possess key advantages of (i) high power densities at relatively low operating temperatures (∼60−120 °C) as well as (ii) portability and light weight, as compared with other fuel cell systems. Moreover, liquid methanol can be safely and inexpensively stored and can also be facilely transported, as compared with other traditional fuels, for example, gaseous hydrogen. Hence, not surprisingly, DMFCs are applicable for a large range of power applications.[5−8]

Metallic platinum is commonly used as a cathodic catalyst, that is, the catalyst for the oxygen reduction half-cell reaction (ORR) in low-temperature fuel cells. However, the generally high cost and the limited global abundance of platinum represent significant barriers to the widespread use of these types of fuel cells. On the other hand, palladium possesses physical properties very similar to those of platinum, including an *fcc* crystal structure and a similar atomic size as well as electronic configuration, and yet, it is much less costly than Pt. Hence, Pd is considered to be a good substitute for Pt as a catalyst in fuel cells.[9,10] As ORR catalysts have evolved, electroactive Pd, in general, and Pd-based alloy catalysts, more specifically, have been proposed as cathode materials for ORR in acidic media,[11,12] because Pd possesses an ORR activity relatively close to that of Pt, among various metals.

Among a number of alloys studied, Pd−Ni catalysts in particular have received significant attention over the years because of the reasonable abundance, low cost, and relative nontoxicity of Ni. In fact, catalytic hydrogenation reactions have been known to improve as a result of adding Ni to Pd,

Received: January 27, 2014
Revised: May 15, 2014
Published: July 2, 2014

   dx.doi.org/10.1021/cs500125y | ACS Catal. 2014, 4, 2544−2555

partly because of the electronic modification of Pd by surrounding Ni atoms.[13] From a theoretical perspective, DFT calculations performed on binary transition metal surface alloys had shown that by doping in Ni, there would be a perceptible downshift of the Pd weighted *d*-band center, which would thereby weaken the binding of oxygen to Pd within this architecture as compared with bare Pd alone.[14] Such a favorable effect originates from (A) the compressive strain induced by the incorporation of Ni atoms into the Pd lattice and (B) a ligand effect arising from the electronic interaction between the Pd atoms and the Ni atoms. Furthermore, as observed from the alloy phase diagram, Pd and Ni form a homogeneous solid solution with a face-centered cubic structure at all compositions and within a large range of temperatures,[15] which renders their synthesis relatively facile.

Accordingly, over the years, it has been verified from the perspective of both kinetic[16] studies and data on actual catalytic performance[17−19] that Pd−Ni is a viable and effective ORR catalyst candidate. For instance, Ramos-Sanchez et al.[20] have reported that the incorporation of less electronegative Ni shifted the onset potential for the ORR by ∼110 mV to more positive values, and at 0.5 mA/cm^2, the cathode overpotential was reduced by 260 mV as compared with Pd alone in a 0.5 M H_2SO_4 solution at 25 °C. Moreover, a hierarchical architecture of Pt-coated PdNi catalyst was observed to have possessed the highest ORR activity as compared with pure Pt/C, Pd/C, and PdNi/C catalysts.[21] Similarly, Pt∼$PdNi_6$ core−shell nanoparticles, measuring ∼20 nm in diameter, not only possess an activity that is 7-fold higher than the state-of-the-art Pt/C but also exhibit excellent long-term electrochemical stability.[22] As an additional plausible explanation for the enhanced performance experimentally noted in these Pd-based binary systems, Tarasevich et al.[23] proposed that the presence of the second metal (i.e., Ni) alloyed with Pd can potentially influence catalytic activity in two ways: namely, (i) through the stabilization of Pd nanoparticles and (ii) by hindering palladium oxide formation.

Recently, our group has developed a class of electrochemically active single-crystalline, one-dimensional (1-D) nanostructures. In general, 1-D materials possess high aspect ratios, fewer lattice boundaries, longer segments of smooth crystal planes, and a relatively low number of surface defect sites, all of which are desirable attributes for fuel cell catalysts.[24−28] In this context, the performance of binary Pd-based alloys (i.e., $Pd_{1-x}Au_x$ and $Pd_{1-x}Pt_x$) toward ORR and the methanol oxidation reaction (MOR) has been dramatically improved by tailoring the morphology, size, and chemical composition. As a salient example,[29] we have recently demonstrated that optimization of size and composition in "Pt-free" Pd_9Au NWs can lead to a measured ORR activity of 0.49 mA/cm^2, which represents more than a 2-fold improvement over commercial Pt NP/C catalysts. For PdAu systems, our studies showed that the enhanced performance likely arises from the structural and electronic properties associated with their alloy-type structure and not simply as a result of the coincidental physical presence of interfacial Pd−Au pair sites.[30]

Ultrathin 1-D structures incorporate the merits of extended, smooth facets associated with an anisotropic morphology along with high surface-area-to-volume ratios due to their nanometer-scale dimensions, all of which combine to give rise to highly promising functional attributes for these materials as electrocatalysts. Not surprisingly, excellent enhancements have also been noted with ultrathin, core−shell Pt∼$Pd_{1-x}Au_x$ NWs,[30] wherein the mutual benefits of the 1D morphology and ultrathin size are merged with a hierarchical structural motif. After the ensuing deposition of a Pt monolayer, a volcano-type composition dependence was observed in the ORR activity values of the Pt∼$Pd_{1-x}Au_x$ NWs as the Au content is increased from 0 to 30% with the activity of the Pt∼Pd_9Au NWs (0.98 mA/cm^2, 2.54 A/mg_{Pt}), representing the optimum performance.

However, in the prior literature, there have been very few reports of ultrathin Pd-based alloys incorporating inexpensive and abundant first-row transition metal dopants. Moreover, the relationship between composition and the corresponding ORR activity has yet to be systematically analyzed. Therefore, in this current study, we have developed an ambient surfactant-based synthetic approach for preparing ultrathin Pd-based NWs wherein the electrochemical activity is controllably increased by substituting Pd atoms for more abundant and less expensive first-row transition metals. Moreover, the distinctive novelty of our work is associated with (a) a comprehensive study of the composition-activity relationship of Pd−Ni binary catalysts, (b) an analysis of the methanol tolerance abilities of nanowires possessing optimized chemical composition, and (c) the feasibility of employing our as-processed ultrathin nanowires as the template for subsequent Pt monolayer deposition toward the development of a highly stable and durable anisotropic core−shell catalytic platform.

In terms of tangible results, our high-quality, carbon-supported Pd−Ni nanowires possessing ultrathin 2 nm diameters were found to maintain a "volcano-type" dependence, as well, with respect to chemical composition, wherein the $Pd_{0.90}Ni_{0.10}$ NW/C composite represented the peak activity among the series of samples analyzed. Moreover, 85% of its original activity was preserved in an electrolyte containing a relatively high 4 mM methanol concentration, implying a correspondingly high methanol tolerance ability. In addition, we were able to test the electrochemical properties of $Pd_{0.90}Ni_{0.10}$ nanowires possessing a Pt monolayer shell. Our results demonstrate outstanding ORR performance with a measured specific activity and platinum mass activity of 0.62 mA/cm^2 and 1.44 A/mg_{Pt}, respectively. Finally, after 10000 cycles of durability testing under realistic simulated conditions, the corresponding specific activity of our as-prepared Pt∼$Pd_{0.90}Ni_{0.10}$ electrocatalyst actually increased by more than 20% from 0.62 mA/cm^2 to 0.76 mA/cm^2.

2. EXPERIMENTAL SECTION

2.1. Synthesis. Unsupported ultrathin Pd−Ni nanowires have been prepared utilizing a modified procedure previously reported by Teng et al.[31] Briefly, in a typical synthesis experiment, palladium(II) nitrate (Alfa Aesar, 99.9%), nickel(II) chloride (Fisher Scientific, >96%), octadecylamine (ODA, 400 mg, Acros Organics, 90%), and dodecyltrimethylammonium bromide (DTAB, 60 mg, TCI, >99%) were dissolved in 7 mL of toluene under vigorous magnetic stirring. The amounts of two metallic precursors were correlated with the desired atomic ratios of these two elements, and the total amount was fixed at 0.056 mmol. For example, to obtain a chemical composition of $Pd_{0.75}Ni_{0.25}$, the amount of palladium(II) nitrate was 0.042 mmol, whereas the amount of nickel(II) chloride was 0.014 mmol.

The entire mixture was brought under an argon atmosphere, utilizing standard air-sensitive Schlenk-line procedures, and was subsequently sonicated for 20 min. Separately, solid sodium

dx.doi.org/10.1021/cs500125y | ACS Catal. 2014, 4, 2544−2555

borohydride (13 mg, Alfa Aesar, 98%) was dissolved into 2 mL of deoxygenated distilled water, and the solution was added dropwise into the precursor mixture while stirring. After 1 h, the reaction mixture was diluted with 2 mL aliquots of distilled water and chloroform, thereby resulting in the separation of the organic and aqueous phases. The black organic phase containing the desired nanowires was then isolated, diluted with 10 mL of absolute ethanol, and eventually centrifuged for 10 min, ultimately resulting in the precipitation of a black solid. The black solid was subsequently washed several times with ethanol and allowed to dry in air.

Adsorption of these as-prepared nanowires onto conductive carbon support (Vulcan XC-72, Cabot) was achieved by first dispersing the isolated black solid, containing a mixture of Pd nanowires and residual surfactant into 6 mL of chloroform, until a homogeneous black mixture was formed. An equal mass of Vulcan carbon (i.e., ∼6 mg) was then added to this mixture, and the mixture was subsequently sonicated for 30 min in a bath sonicator. As-prepared composites were then isolated by centrifugation and fixed onto the carbon substrate by immersion in hexanes for 12 h. Excess ODA and DTAB were removed by washing the powder several times with hexanes and ethanol.

2.2. Activation of Pd−Ni Nanowires. The removal of residual adsorbed ODA surfactant was accomplished by a two-step protocol. In the first step, a surface ligand exchange was performed by dispersing the as-prepared composites into *n*-butylamine (Acros Organics, +99.5%) by sonication, and the resulting dispersion was stirred for a period of 3 days to ensure complete exchange of the ODA with the butylamine. The treated product was subsequently isolated by centrifugation and washed with ethanol to remove excess butylamine.

In the second step, the butylamine ligands and other organic impurities were removed by a selective CO adsorption process previously described by one of our groups.[32] Briefly, the supported nanowires were deposited onto a glassy carbon electrode (c.f., section 2.4), and the potential was cycled in deoxygenated 0.1 M $HClO_4$ up to a potential of 1.3 V at a rate of 100 mV/s until a stable profile was obtained. Thereafter, the electrode was immersed in a CO-saturated electrolyte for 30−45 min so as to selectively displace residual organic impurities from the surfaces of the NWs. The electrode was then washed in ultrapure water and transferred to a freshly deoxygenated electrolyte, wherein a CO stripping cyclic voltammogram (CV) was obtained by cycling the potential up to 1.15 V. The CO adsorption/stripping process was ultimately repeated an additional two times or until the CO stripping profile was deemed to be reproducible.

Regarding the commercial Pt nanoparticle (NP) /C samples, we employed a previously reported pretreatment protocol[29,30,33] not only to successfully remove any trace organic impurities but also to preserve the intrinsic size and morphology of the nanoparticles themselves. Specifically, the Pt NP/C controls were treated by cycling between 0 and 1.0 V (versus RHE) in 0.1 M $HClO_4$ until a stable CV profile was achieved.

2.3. Structural Characterization. X-ray diffraction (XRD) measurements were performed using a Scintag diffractometer. Patterns were typically collected over 35−95° in the Bragg configuration with a step size of 0.25° using Cu Kα radiation (λ = 1.5415 nm). TEM images and energy dispersive X-ray spectroscopy data collected in scanning TEM mode (TEM-EDAX) were obtained on a JEOL 1400 transition electron microscope equipped with a 2048 × 2048 Gatan CCD camera at an accelerating voltage of 120 kV. To improve the signal-to-noise in general, the EDAX spectral background was effectively eliminated by subtracting the signal attributed to the blank regions on the TEM grid from the desired response of the actual samples. In so doing, signals associated with the Cu peak (originating from the Cu grid) and the Fe peak (intrinsically incorporated within the sample holder) were essentially removed, thereby allowing for the unambiguous observation and interpretation of the highlighted Ni peak. High-resolution transmission electron microscopy (HRTEM), high angle annular dark field images (HAADF), and selected area electron diffraction (SAED) patterns were collected on a JEOL 2100F analytical transmission electron microscope equipped with a Gatan CCD camera and a Gatan HAADF detector and operating at an accelerating voltage of 200 kV.

Thermogravimetric analysis was performed using a TGA Q500 (TA Instruments) on dried aliquots of the catalyst ink to estimate the total metal content. Isotherms were obtained by raising the temperature from 25 to 900 °C at a rate of 10 °C/min under a flow of extra-dry air provided at a rate of 60 mL/min. The mass profiles confirmed that the carbonaceous material (e.g., Vulcan XC-72R and residual organic surfactants) was entirely removed once a threshold level of 600 °C had been achieved. On the basis of two separate experiments, TGA measurements established that the combined Pd and Ni loading was 14.9 ± 1.2%.

2.4. Electrochemical Characterization. Prior to electrochemical characterization, as-prepared isolated nanowires were rendered into catalyst inks by dispersing the dry powders into ethanol so as to create an approximately 2 mg/mL solution. Before application of the nanowire ink, a glassy carbon rotating disk electrode (GC-RDE, Pine Instruments, 5 mm) was polished until a pristine finish was obtained. Then the electrode was modified by drying two 5 μL drops of the dispersed catalyst ink onto the surface and allowing them to dry in air. Once dry, the electrode was sealed with one 5 μL drop of an ethanolic 0.025% Nafion solution prepared from a 5% stock solution (Aldrich). Electrochemical measurements were obtained in a 0.1 M perchloric acid (Fisher Scientific, Optima grade) solution prepared using high-purity type 1 water possessing a high resistivity of 18.2 MΩ·cm. A Ag/AgCl (3 M Cl^-) combination isolated in a double junction chamber (Cypress) and a platinum foil served as the reference electrode and the counter electrode, respectively. All of the potentials in this paper have been reported with respect to the reversible hydrogen electrode (RHE) unless otherwise mentioned.

In addition to a Pd−Ni nanoscale alloy, a Pt∼PdNi core−shell structure was also prepared through a two-step Pt deposition method, and its electrochemical properties were investigated thereafter. Specifically, after CO stripping was performed, a monolayer of Cu was deposited onto the surface of $Pd_{0.90}Ni_{0.10}$ NWs by Cu underpotential deposition (UPD) from a deoxygenated solution of 50 mM $CuSO_4$, maintained in a 0.10 M H_2SO_4 electrolyte.[34] The Cu monolayer-modified electrode was then transferred to a solution of 1.0 mM K_2PtCl_4 solution in 50 mM H_2SO_4 for several minutes. The Pt-monolayer-modified electrode was subsequently removed from the cell and rinsed thoroughly before ORR measurements were performed.

The measurement of the ORR performance of the various catalyst samples was carried out by employing a thin-layer rotating disk electrode method, a protocol recently reviewed in

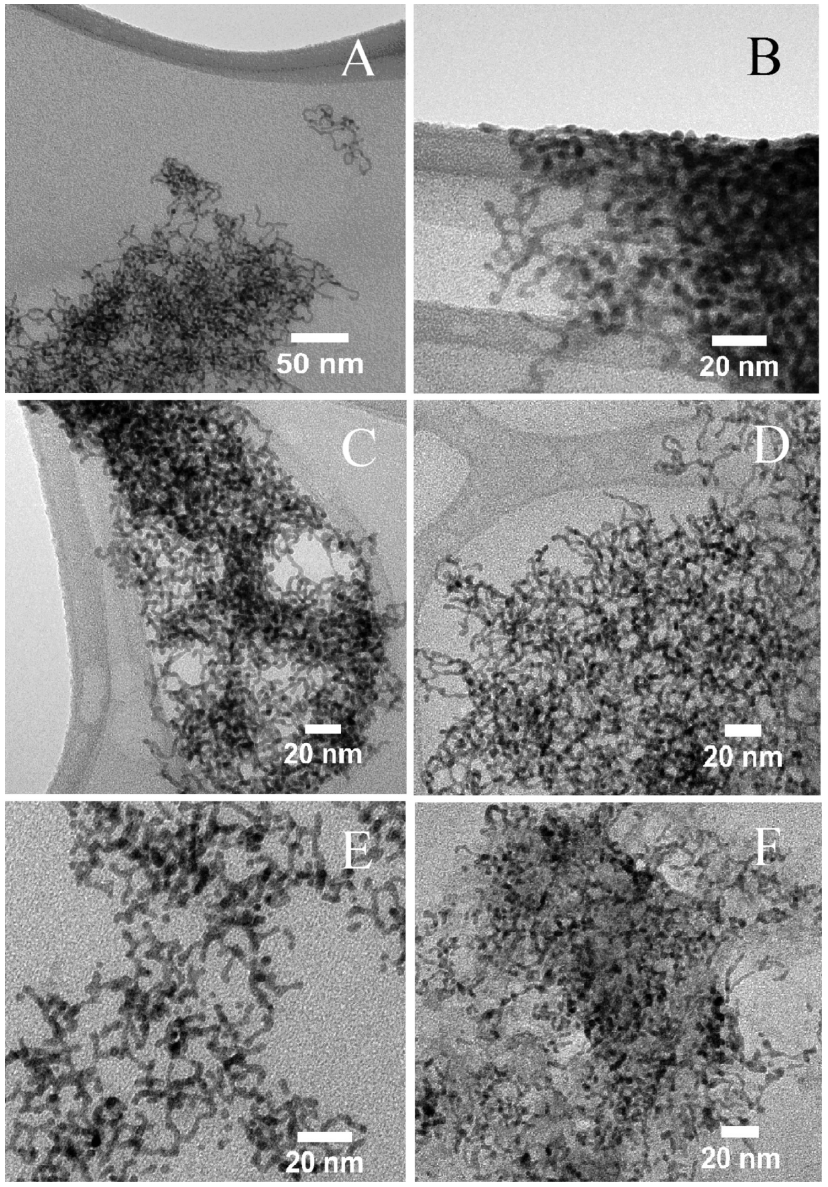

Figure 1. Representative TEM images of as-prepared (A) Pd, (B) $Pd_{0.90}Ni_{0.10}$, (C) $Pd_{0.83}Ni_{0.17}$, (D) $Pd_{0.75}Ni_{0.25}$, (E) $Pd_{0.60}Ni_{0.40}$, and (F) $Pd_{0.50}Ni_{0.50}$ free-standing ultrathin nanowires.

detail by Kocha and co-workers.[35] First, CVs were obtained in deoxygenated electrolyte at a scan rate of 20 mV/s so as to establish the electrochemically accessible surface area (ESA). The ESA is calculated in this case by converting the average of the hydrogen adsorption (H_{ads}) and desorption (H_{des}) charge (after correcting for the double layer) into a real, actual surface area by utilizing 210 $\mu C/cm^2$ as a known conversion factor. For Pt~Pd and Pt~$Pd_{0.90}Ni_{0.10}$ samples, the ESA was computed by averaging the H_{ads} and the Cu UPD charge values to achieve a more accurate and representative estimate of the electrochemical surface area (Supporting Information (SI) Table S1).[36,37] Then, the ORR activity of the various catalyst samples was measured by obtaining polarization curves in oxygen-saturated electrolytes at 20 °C with the electrode rotated at a rate of 1600 rpm and the potential scanned at a rate of 10 mV/s. The kinetic current density was calculated from the Koutecky–Levich relationship, and it was then normalized to either the ESA or the platinum mass of the catalyst loaded onto the GCE to determine either the surface area or mass normalized kinetic current (J_k) densities. Each experiment was performed up to three times to confirm reproducibility of results. The reported specific and Pt mass activities, described quantitatively in SI Table S2, represent an average value obtained from activities measured on several separately prepared electrodes.

Durability testing was conducted on Pt~$Pd_{0.90}Ni_{0.10}$ electrocatalysts under half-cell conditions in perchloric acid by utilizing a durability test protocol standard, previously described by the U.S. Department of Energy[38] for simulating a catalyst lifetime under realistic membrane electrode assembly operating conditions. Specifically, the potential was cycled from 0.6 to 1.0 V in an acidic 0.1 M $HClO_4$ medium and left open to the atmosphere. Data on ESA and the corresponding electrochemical surface area activity were obtained after every 5000 cycles.

dx.doi.org/10.1021/cs500125y | ACS Catal. 2014, 4, 2544−2555

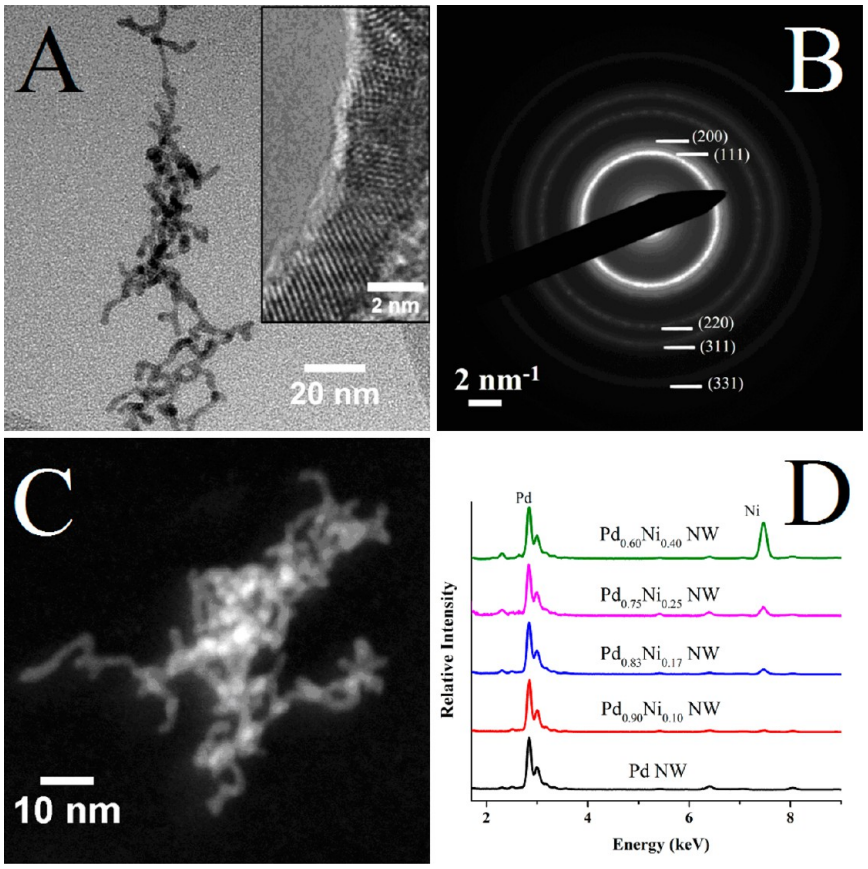

Figure 2. (A) Representative TEM image of $Pd_{0.90}Ni_{0.10}$ NWs supported on Vulcan XC-72R carbon support. The inset shows a high resolution TEM image, highlighting the segmented nature of the individual nanowire. (B) The SAED pattern obtained from a set of NWs is shown. (C) An HAADF image taken from a representative aggregate of $Pd_{0.90}Ni_{0.10}$ NWs is presented. (D) Characteristic EDAX spectra have been collected from a series of Pd−Ni NW composites of various chemical compositions.

3. RESULTS AND DISCUSSION

3.1. Synthesis and Structural Characterization of Pd−Ni Nanowires with Various Chemical Compositions. We employed an ambient, surfactant-based technique to synthesize Pd−Ni ultrathin nanowires with a diameter of ∼2 nm. This synthetic approach has been previously used to yield long, extended polycrystalline nanowires, which possess lengths of several tens of nanometers and consist of single crystalline constituent segments.[30−32] Specifically, appropriate metal precursors (namely, Pd^{2+} and Ni^{2+}) were reduced by sodium borohydride ($NaBH_4$) in the presence of octadecylamine (ODA) and *n*-dodecyltrimethylammonium bromide (DTAB), serving as surfactant and phase transfer agent, respectively, to create thermodynamically unstable, elongated primary nanostructures (PNs). The secondary growth of these PN "nuclei" along preferred growth directions, including the (111) direction, leads to the formation of thread-like nanowire networks.[31] This synthetic protocol has enabled us to tune chemical composition. The stoichiometry of the NW can be directly altered by modifying the corresponding stoichiometric ratio of the metallic precursors within the precursor solution. In this case, Pd−Ni nanowire samples can be routinely and controllably prepared with chemical compositions ranging from $Pd_{0.90}Ni_{0.10}$ to $Pd_{0.50}Ni_{0.50}$.

X-ray powder diffraction (XRD) obtained on the series of as-prepared Pd−Ni nanowires (SI Figure S1) has revealed that the NWs are composed of homogeneous alloys with a face-centered cubic (fcc) crystal structure. We did not observe any obvious peaks associated with either the metallic nickel or nickel oxides observed, thereby suggesting the incorporation of Ni atoms within the fcc structure of Pd. Nonetheless, on the basis of studies that involve a cross-sectional composition analysis of Pd− or Pt−Ni nanostructures, it is possible that though the valence of Ni in the core region is 0, the Ni on the surface may actually exist as a form of oxide, such as NiO or $Ni(OH)_2$ as a result of the presence of surface oxidation.[22,39] Therefore, it is likely that our as-prepared nanostructures possess a variant of nickel oxide on their surface, as well. Nevertheless, the patterns of the peaks can be attributed to the elemental Pd phase with a slight shift toward higher 2θ angle, indicating possible lattice contraction. Such a phenomenon reflects a partial substitution of Pd atoms with Ni atoms, which possess a smaller atomic radius. Because of a broadening of the peaks, which likely originates from the small crystallite size, calculations of lattice parameters based on XRD patterns tend to be difficult and, hence, could be somewhat imprecise. Consequently, lattice parameters were more precisely determined by analyzing the corresponding selective area electron diffraction (SAED) patterns, as discussed later.

Transmission electron microscopy (TEM) was employed to examine the morphology, crystallinity, and uniformity of a series of as-prepared Pd−Ni nanowires. As shown in Figure 1, the overall structure of the samples with >60 atom % Pd consists of discrete individual one-dimensional nanowires clustered together as part of a larger three-dimensional aggregated network. To the best of our knowledge, in the

dx.doi.org/10.1021/cs500125y | ACS Catal. 2014, 4, 2544−2555

past, this specific synthetic protocol has been applied only to noble metals and noble metal alloys, namely, Pt, Pd, and Au. In addition, it is proposed that the growth mechanism involves the surfactant-directed assembly of discrete anisotropic seed nanocrystals into elongated nanowires composed of individual segments. An analogous way of describing this growth mechanism, especially for ultrathin nanowires, is that it can be viewed as not only ligand-controlled but also associated with an oriented attachment of nanoparticulate building blocks.[26] This unique growth mechanism renders the reaction process itself sensitive to the presence of oxygen, which can selectively adsorb onto and etch the edges of the growing nanowire, thereby leading to shorter nanorods in the presence of dissolved O_2 and longer nanowires in the absence of O_2.[31] Thus, it is not surprising that the introduction of non-noble metals, for example, Ni, which are much more prone to oxidation than their noble metal counterparts, may likely hinder the assembly of constituent substructural seeds. Moreover, the higher the content of Ni, the more difficult the assembly process, and hence, the more challenging the resulting nanowire formation is.

A high-resolution TEM (HRTEM) image (inset of Figure 2A) revealed that the NWs are actually polycrystalline and are composed of multiple single crystalline segments, as we had expected on the basis of previous work.[29,30,32] The selected area electron diffraction (SAED) pattern shown in Figure 2B highlights the likelihood of such structure by showing not only continuous rings that can be indexed to the (111), (200), (220), (311), and (331) reflections for the calculated fcc $Pd_{0.90}Ni_{0.10}$ alloy but also discrete diffraction spots, indicative of the high degree of crystalline substructure. Therefore, on the basis of the collected electron diffraction data, the $Pd_{0.90}Ni_{0.10}$, $Pd_{0.83}Ni_{0.17}$, and $Pd_{0.75}Ni_{0.25}$ NWs were experimentally determined to possess lattice parameters of 3.856, 3.836, and 3.796 Å, respectively, which are in agreement with the calculated values of 3.861, 3.831, and 3.806 Å for the respective alloys.

Theoretical calculations generated by utilizing a reliable software package, that can calculate phase diagrams, have shown that $Pd_{1-x}Ni_x$ tends to form a homogeneous alloy with an fcc structure under ambient conditions wherein "x" is no greater than 0.7 (SI Figure S2).[40] In other words, for all of the sample compositions synthesized herein, the corresponding alloys should possess a homogeneous chemical structure. Indeed, the XRD and HRTEM data collectively suggest that our as-prepared $Pd_{1-x}Ni_x$ NWs are, in fact, uniform and homogeneous, because no diffraction data or other compelling evidence were observed for the formation of either Pd, Ni, or their related oxides.

We have also used a high angle annular dark field (HAADF) imaging technique, which is sensitive to atomic number (Z), to further examine the homogeneity of chemical composition along the lengths of our as-prepared wires. Figure 2C shows a representative HAADF image collected from a typical $Pd_{0.90}Ni_{0.10}$ sample. The largely uniform contrast observed over the collection of individual discrete NWs present is suggestive of a high degree of homogeneity of chemical composition. The brighter contrast at the center of the collection and within some spherical areas can be attributed to signals emanating from physically overlapping nanowires as well as from discrete interconnects among the NW segments. Such an observation has also been noted in analogous Pd_9Au NWs in previous reported work from our group.[30] Although it is beyond the scope of this report, we intend to further examine the structure and chemical composition of our $Pd_{1-x}Ni_x$ NWs, utilizing techniques such as X-ray absorption spectroscopy.

Representative point EDS spectra, corresponding to the elemental composition of areas measuring as small as several square nanometers, were collected over multiple locations for all of our as-prepared 1-D nanostructures, and these are shown in Figure 2D. The diameters of various as-prepared $Pd_{0.90}Ni_{0.10}$, $Pd_{0.83}Ni_{0.17}$, $Pd_{0.75}Ni_{0.25}$, $Pd_{0.60}Ni_{0.40}$, and $Pd_{0.50}Ni_{0.50}$ nanostructures along with their actual chemical compositions obtained thorough EDAX analysis are summarized in Table 1. The small deviation in both diameter and atomic composition observed validates the idea of a high uniformity of these as-prepared nanowires in terms of both (a) morphology and (b) Pd and Ni content.

Table 1. Summary of the Morphologies, Diameters, And Actual Chemical Compositions, As Determined by EDAX Analysis, of As-Prepared Pd−Ni Nanowires with Various Pd/Ni Molar Ratios

precursor metal composition	morphology	diameters (nm)	actual composition (Pd/Ni, molar ratio)[a]	standard deviation of chemical composition[a]
$Pd_{0.90}Ni_{0.10}$	wires	2.7 ± 0.3	$Pd_{0.92}Ni_{0.08}$	0.02
$Pd_{0.83}Ni_{0.17}$	wires	2.3 ± 0.2	$Pd_{0.84}Ni_{0.16}$	0.04
$Pd_{0.75}Ni_{0.25}$	wires	2.1 ± 0.3	$Pd_{0.77}Ni_{0.23}$	0.03
$Pd_{0.60}Ni_{0.40}$	short wires	2.4 ± 0.2		
$Pd_{0.50}Ni_{0.50}$	short wires/ segments	2.3 ± 0.4		

[a]Chemical compositions of $Pd_{0.60}Ni_{0.40}$ and $Pd_{0.50}Ni_{0.50}$ short wires were not precisely examined because these materials were not used in subsequent electrochemical tests.

Regarding electrochemical characterization, our main focus has been directed to $Pd_{0.90}Ni_{0.10}$, $Pd_{0.83}Ni_{0.17}$, and $Pd_{0.75}Ni_{0.25}$ because, on the basis of prior reports involving Pd−Ni nanoparticles,[17,41] they represent promising candidates for ORR. Our nanowire samples maintained chemical compositions that were rather close to the expected values with a minimal deviation of 3% from batch to batch. Specifically, the actual compositions of these three nanostructures were deemed to be $Pd_{0.92}Ni_{0.08}$ (±0.02), $Pd_{0.84}Ni_{0.16}$ (±0.04), and $Pd_{0.77}Ni_{0.23}$ (±0.03), respectively.

3.2. Electrochemical Properties and ORR Performance of Pd−Ni Nanowire Series. In prior studies from our group, a treatment protocol was developed for the removal of residual organic impurities from the surfaces of analogous ultrathin Pd nanowires, which combined (i) a UV−ozone atmosphere pretreatment with (ii) a selective CO adsorption process.[29,30,32] In this specific case, however, we have developed our two-step protocol to include a more facile and potentially "greener" pretreatment process involving a simple surface-capping ligand substitution with butylamine. In previous reports, ligand substitution reactions were effectively employed to remove a mixture of a borane-*tert*-butylamine complex and hexadecanediol from the surfaces of Pt_3Ni nanoparticles, for instance.[42] Herein, the ligand substitution was accomplished by dispersing as-synthesized ODA-capped PdNi alloy nanowires into pure butylamine for a period of 3 days under completely ambient conditions. The subsequent butylamine-capped nanowires could be activated toward a selective CO-adsorption process, which is capable of displacing organic capping ligands with alkyl

dx.doi.org/10.1021/cs500125y | ACS Catal. 2014, 4, 2544−2555

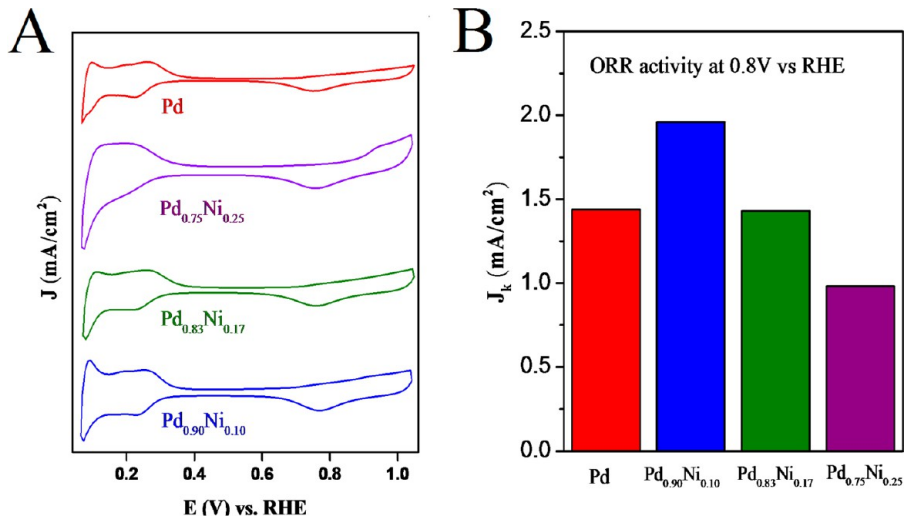

Figure 3. (A) Cyclic voltammograms obtained from a series of butylamine-treated ultrathin Pd−Ni NWs by comparison with elemental Pd NWs. (B) The corresponding experimentally calculated area-normalized kinetic current densities (J_k, mA/cm^2).

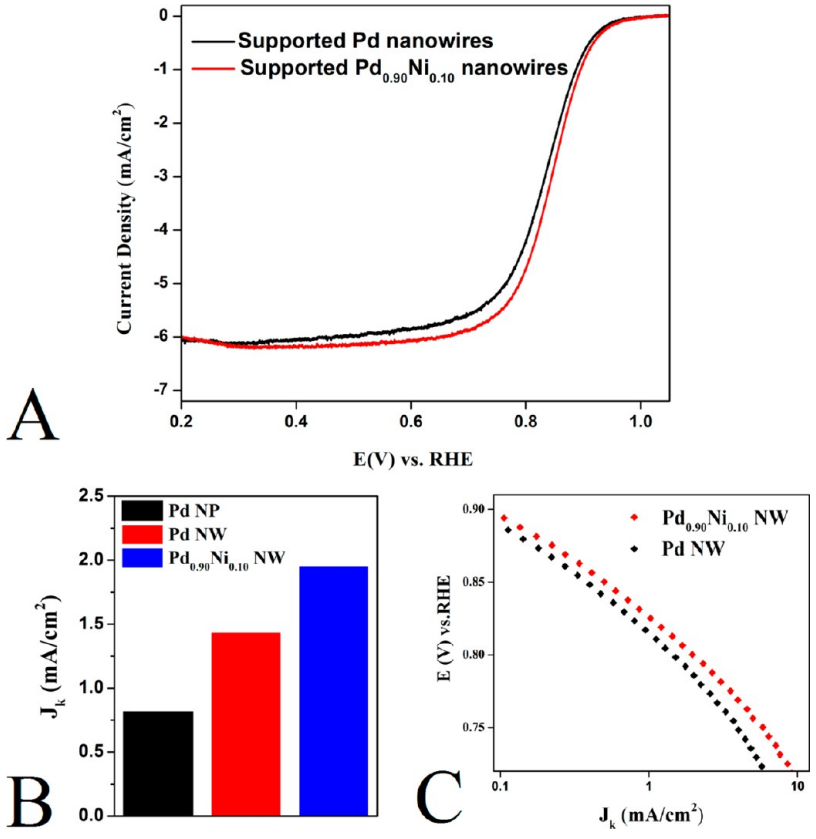

Figure 4. (A) Representative polarization curves obtained from $Pd_{0.90}Ni_{0.10}$ NWs with analogous Pd NWs serving as a comparison. (B) Data on specific activities (mA/cm^2) of $Pd_{0.90}Ni_{0.10}$ nanowires, elemental Pd nanowires, and commercial Pd nanoparticles. (C) A potential versus specific activity plot (E versus J_k) for these two nanowires.

chains of up to six carbons in length.[29,30,43] That is, we have demonstrated that the selective CO stripping process alone is not capable of fully removing the ODA; however, in combination with a ligand substitution reaction using the 4-carbon butylamine molecule, the selective CO adsorption process can successfully produce electrochemical features in the CV profile associated with pristine Pd nanostructures, while at the same time, conserving its overall wire morphology (SI Figure S3).

The cyclic voltammograms along with the associated specific ORR activities measured at 0.8 V are displayed in Figure 3A and B. As compared with elemental palladium, the onset potentials for the oxide species in the cyclic voltammograms of the Pd−Ni series have been shifted to lower potentials, an observation that is consistent with the incorporation of Ni into the Pd-based alloy, thereby leading to a lower overall potential for the onset of surface oxide formation. Moreover, the positions of the oxide reduction peaks in Pd−Ni CVs shifted

dx.doi.org/10.1021/cs500125y | ACS Catal. 2014, 4, 2544−2555

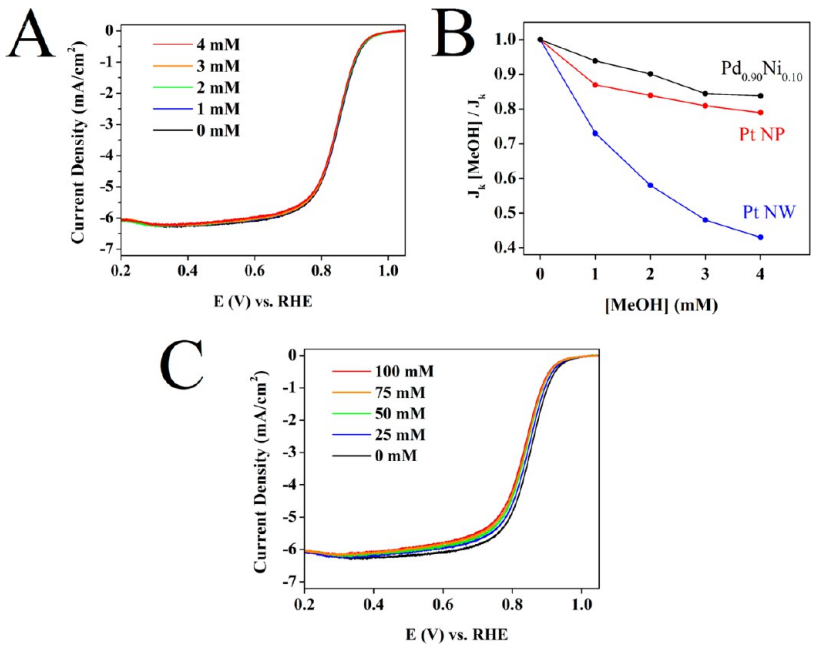

Figure 5. Probing the methanol tolerance capability of as-processed $Pd_{0.90}Ni_{0.10}$ NWs. Polarization curves were obtained in the presence of various methanol concentrations, ranging from 0 to 4 mM. (A) A plot of the ratio of the specific activity values measured in the presence of methanol (J_K [MeOH]) to that measured in pure electrolyte (J_K) as a function of increasing methanol concentration (B) for $Pd_{0.90}Ni_{0.10}$ NWs, with both Pt NWs and commercial Pt NP/C serving as controls. (C) Polarization curves obtained from $Pd_{0.90}Ni_{0.10}$ in 0.1 M $HClO_4$ with increasing methanol concentrations of 25, 50, 75, and 100 mM, respectively.

toward higher potential (relative to Pd) as a result of the "ligand effect" arising from the Ni content. This could be rationalized by the Nørskov–Hammer theory, which implies that Ni as a dopant withdraws electron density away from Pd, thereby weakening the interaction between Pd itself and the resulting oxide species. Interestingly, however, $Pd_{0.90}Ni_{0.10}$ shows the largest shift (769.3 mV as compared with 752.2 mV for elemental Pd), followed by $Pd_{0.83}Ni_{0.17}$ (759.8 mV) and, finally, $Pd_{0.75}Ni_{0.25}$ (755.2 mV).

We attribute such observations to the combination of the Ni doping effect and the oxophilic nature of Ni atoms themselves. In essence, the doping effect or "ligand effect" should imply a direct proportional relationship between the amount of dopant and the magnitude of the shift in the oxide reduction peak. However, this is only true with a small quantity of dopant. In fact, when the molar percentage of the non-noble metal exceeds a certain value (in this case, 10% of Ni), the oxophilicity of nickel was a more significant factor than the ligand effect, thereby rendering the wire structure more prone to oxidation. Nonetheless, deducing the exact relationship between the amount of Ni dopant present and the oxide reduction peak position is beyond the scope of this research, and a more thorough investigation involving probing of the Pd electronic structure will need to be conducted for this issue to be properly resolved.

As Figure 3B has shown, the activities of the series (including elemental Pd) exhibited a "volcano"-shaped trend in which the highest activity was provided by the $Pd_{0.90}Ni_{0.10}$ sample, namely, at 1.96 mA/cm^2 measured at 0.8 V. A direct comparison of the specific activities of our supported $Pd_{0.90}Ni_{0.10}$ and elemental Pd nanowires is shown in Figure 4. On the basis of the polarization curves obtained in an oxygen-saturated electrolyte (Figure 4A), the $Pd_{0.90}Ni_{0.10}$ NWs possess significantly enhanced performance, especially as compared with elemental Pd NWs and commercial Pd NP/C (Figure 4B). Moreover, the potential versus specific activity (E versus J_k) plot (Figure 4C) further confirms the consistently improved performance of $Pd_{0.90}Ni_{0.10}$ nanowires with respect to analogous elemental Pd nanowires over a broad range of plausible fuel cell potentials. The polarization curves of the remaining nanowire compositions tested, namely $Pd_{0.83}Ni_{0.17}$ and $Pd_{0.75}Ni_{0.25}$, are reported in SI Figure S4.

In prior research studying the utilization of Pd–Ni nanoparticles as ORR electrocatalysts,[41,44] the "optimum composition" was found to be $Pd_{0.60}Ni_{0.40}$. By contrast, we find herein that the $Pd_{1-x}Ni_x$ NW electrocatalysts maintain an optimum performance with a composition of $Pd_{0.90}Ni_{0.10}$. This interesting morphology-dependent finding may have several plausible explanations. First, this difference in behavior can be potentially attributed to a corresponding difference between the surface structure and composition of the Pd–Ni NPs and NWs. Specifically, recent theoretical work has demonstrated that the surface segregation of Pd atoms occurs at the catalytic interface (i.e., the 1–3 uppermost atomic layers) and that the surface composition and structure of the dealloyed surface varies significantly for exposed (111), (100), and (110) facets, respectively.[45] It is typically observed that noble metal NWs possessing diameters measuring 2 nm expose primarily (111) and (100) facets with a relatively low defect site density, whereas the corresponding analogous NPs maintain predominantly (111)-terminated facets with a relatively large density of (110)-type defect sites.[10,46] In addition, the degree of Pd enrichment and the corresponding surface structure are also highly dependent upon the surface strain, which is known to be comparatively different for nanoparticles versus nanowires because of their isotropic and anisotropic geometries, respectively. Hence, on the basis of this theory, we believe that significant differences in the surface structure and strain of the NWs and NPs may lead to differing degrees of surface segregation at the catalytic interface. What we propose herein,

dx.doi.org/10.1021/cs500125y | ACS Catal. 2014, 4, 2544–2555

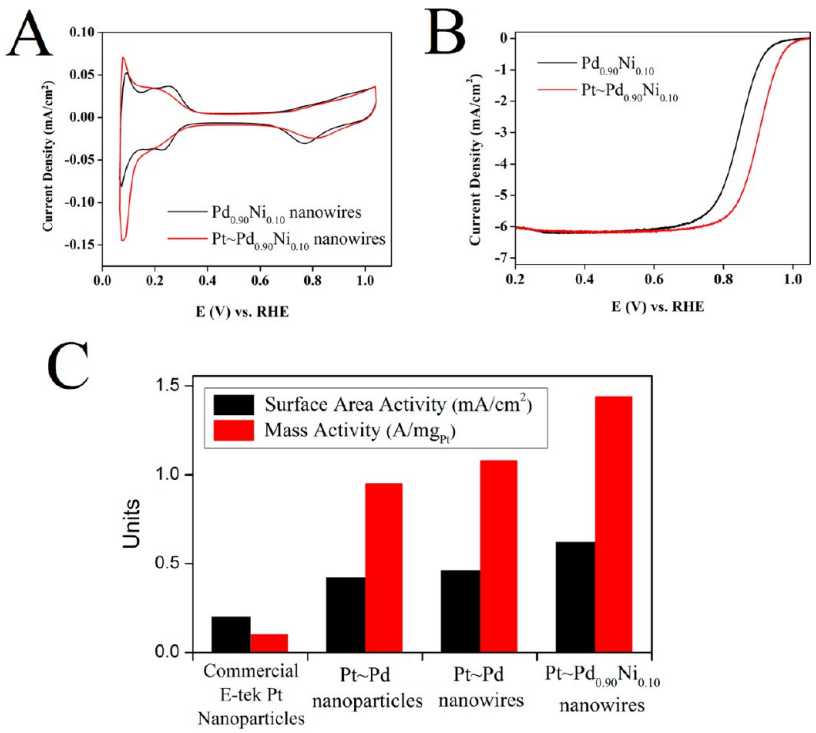

Figure 6. Cyclic voltammograms (A) obtained for $Pd_{0.90}Ni_{0.10}$ nanowires and Pt~$Pd_{0.90}Ni_{0.10}$ core−shell nanowires, in a 0.1 M $HClO_4$ solution at 20 mV/s. (B) The polarization curves for both of these two nanowire composites were obtained using a rotation rate of 1600 rpm in a 0.1 M $HClO_4$ solution at 20 °C. (C) The electrochemical surface area activity and mass activity at 0.9 V for Pt~$Pd_{0.90}Ni_{0.10}$ are shown by comparison with commercial carbon-supported Pt nanoparticles, analogous Pt~Pd nanoparticles, and ultrathin Pt~Pd nanowires, respectively.

therefore, is that as a result of the morphology-dependent Pd enrichment, the surface layers of the reported $Pd_{0.60}Ni_{0.40}$ nanoparticles and of our $Pd_{0.90}Ni_{0.10}$ nanowires likely possess approximately the same chemical composition at the interface and, therefore, a similar "active site" profile, thereby resulting in the comparably favorable ORR activities, experimentally recorded.

Second, as an alternative, complementary explanation for the observed activity enhancement of Pd alloys as compared with Pd alone, it is worth noting, from previous studies,[47,48] that one of the roles of the second metal "dopant", that is, Ni, is to lower the amount of potentially deleterious OH coverage on Pd by inducing lateral repulsion between OH species adsorbed on Pd and neighboring OH or O species adsorbed on Ni. Although this effect is minimal either at low pH or in an acidic environment, the net result of this interaction is to yield a positive shift associated with the formation of OH on Pd or, conversely, the oxidation of PdNi itself. In principle, decreasing OH coverage on Pd should increase the number of free Pd "active" sites.[49] Although it is beyond the scope of this report, additional insights into the physicochemical origins of the enhanced performance can be garnered by techniques such as X-ray absorption and X-ray photoelectron spectroscopies, which can likely provide detailed information concerning surface structure and surface chemical composition. We intend to perform these types of characterization experiments in the future.

In the operation of DMFCs, the migration of methanol from the anodic half-cell to the cathodic half-cell often results in a deactivation of the catalyst. To further prove that our $Pd_{0.90}Ni_{0.10}$ nanowires are promising as actual, practical ORR candidates, we have conducted methanol tolerance experiments. Figure 5A displays polarization curves obtained from $Pd_{0.90}Ni_{0.10}$ NWs in the presence of a range of methanol concentrations (i.e., 0−4 mM). It can be inferred from these data that at these levels, methanol exerts minimal effect on the shape and intensity of the measured polarization curves. A more quantitative analysis (shown in Figure 5B) validates a high methanol tolerance ability for our systems. In fact, our purified $Pd_{0.90}Ni_{0.10}$ NWs maintain a significantly improved tolerance to methanol by maintaining 85% of their initial activity in the presence of 4 mM methanol, which designates a tangible improvement, especially as compared with controls consisting of commercial elemental 0D Pt NP/C (79%) and 1D Pt NWs (43%).

Moreover, Figure 5C shows a minimal difference of 20 mV in half-wave potential for polarization curves obtained in a mixture of 0.1 M $HClO_4$ and 100 mM MeOH solution as compared with an analogous polarization curve obtained in 0.1 M $HClO_4$ solution, thereby corroborating the high methanol tolerance ability of our nanowires. The fact that 55% of the initial activity for our $Pd_{0.90}Ni_{0.10}$ nanowires was retained after these experiments should be considered noteworthy, especially given the fact that commercial Pt nanoparticles likely maintain either little or no ORR activity under identical experimental conditions and protocols. In addition, a comparison of CVs both in the presence of as well as in the absence of methanol, serving as a component of the electrolyte, further highlights that the main defining features of $Pd_{0.90}Ni_{0.10}$ cyclic voltammograms are indeed preserved, even after the addition of methanol (SI Figure S5). Both the polarization curves and CV comparative analysis imply the absence of a CO-poisoning effect on the actual $Pd_{0.90}Ni_{0.10}$ surface which would have been particularly detrimental to ORR performance.

It has been demonstrated in our previous work and many other reports that binary nanostructures, both 0-D[50] and 1-

dx.doi.org/10.1021/cs500125y | ACS Catal. 2014, 4, 2544−2555

D,[29,30] represent a promising platform for the subsequent deposition of a Pt monolayer shell, and hence, one can envision forming core−shell ORR catalysts possessing outstanding performance, yet with a minimum amount of Pt metal. For example, a high-performing catalyst consisting of Pt decorating PdNi nanoparticles supported on carbon black has been shown to evince performance superior to that of analogous pure Pt, Pd, and PdNi, all supported on carbon black.[21] In this current report, we have specifically designed ultrathin Pt~$Pd_{0.90}Ni_{0.10}$ core−shell nanostructures that displayed significant electrochemical improvement as compared with analogous ultrathin Pt~Pd nanowires. The deposition of the platinum monolayer was accomplished by Cu UPD, followed by galvanic displacement of the Cu atoms with $[PtCl_4]^{2-}$.

Cyclic voltammetric comparison of the $Pd_{0.90}Ni_{0.10}$ and Pt~$Pd_{0.90}Ni_{0.10}$ composites (Figure 6A) showed that after Pt deposition, the hydrogen adsorption region resembled that of a nanostructured Pt surface. Moreover, the oxidation and reduction peaks were shifted to higher potentials. All of these observations support the findings from our prior observations.[32] The polarization curves of the corresponding samples are displayed in Figure 6B. We note that the Pt~$Pd_{0.90}Ni_{0.10}$ NWs possessed an ORR onset in the region of 0.9−1.0 V, which is consistent with that of nanostructured Pt catalysts. On the basis of the polarization curves, the specific activities and corresponding Pt mass activities at 0.9 V were measured by comparison with commercial platinum nanoparticles and are shown in Figure 6C. Specifically, the Pt~$Pd_{0.90}Ni_{0.10}$ nanowires yielded area and mass activities of 0.62 mA/cm^2 and 1.44 A/mg_{Pt}, respectively.

Moreover, we have tested the electrochemical durability of our processed Pt~$Pd_{0.90}Ni_{0.10}$ composites under half-cell conditions. Specifically, the electrode was immersed in naturally aerated 0.1 M $HClO_4$ solution while the potential was cycled between 0.6 and 1.0 V to properly simulate the relevant electrochemical environmental conditions associated with ORR feasibly occurring within a functional working fuel cell configuration. On the basis of this protocol, the ESA as well as the specific activities could be independently probed by obtaining cyclic voltammograms (Figure 7A) and polarization curves (Figure 7B) through potential cycling, that is, through an accelerated degradation test (ADT).

We found that the Pt~$Pd_{0.90}Ni_{0.10}$ catalytic architecture maintained 81% and 77% of their initial measured ESA values after 5000 and 10 000 cycles, respectively. This decline in ESA is comparatively more rapid as compared with our analogous Pt~Pd ultrathin nanowires previously reported, which maintained ~100% of ESA after 5000 cycles and 83% after 10 000 cycles. This accelerated ESA loss rate can potentially be attributed to the relative instability of Ni content in our material toward an acidic testing environment, because Ni is generally less inert than Pd and, hence, more prone to dissolution.

In addition, the specific activity, or surface area activity, of Pt~$Pd_{0.90}Ni_{0.10}$ has also been studied as a function of durability. As shown in Figure 7B, despite a nearly 20% of ESA loss, the corresponding specific activity of our as-prepared electrocatalysts actually increased by more than 20% after 10 000 cycles (from 0.62 to 0.76 mA/cm^2). As a matter of record, there was only a 2 mV loss of half-wave potential in the process. This promising result is in excellent agreement with our previous study of both Pt~Pd nanoparticles and Pt~Pd nanowires possessing analogous dimensions.[51,32] We attribute the

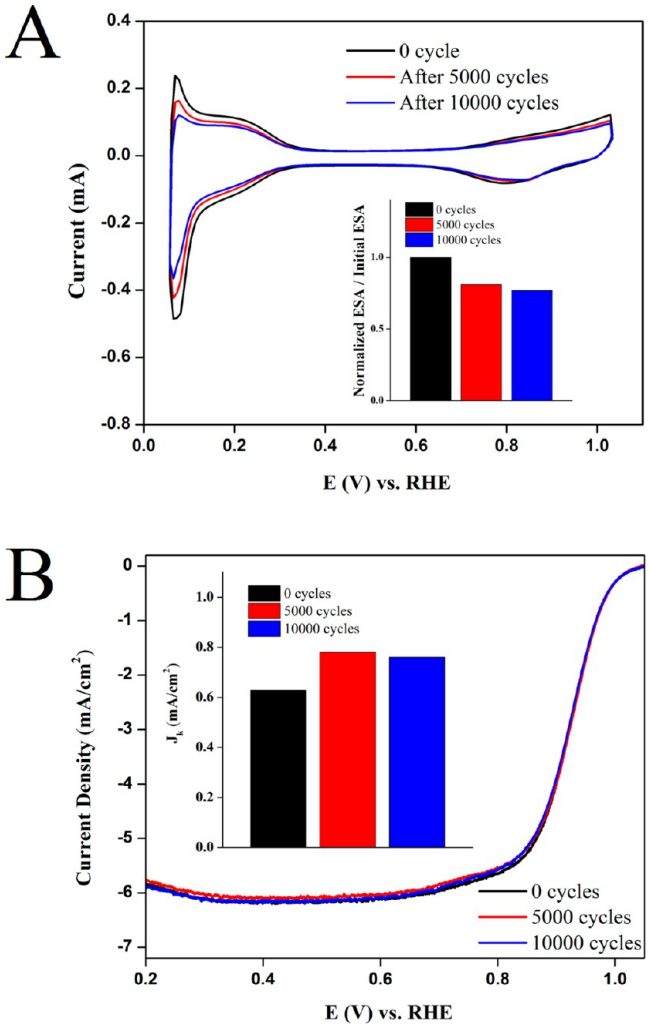

Figure 7. (A) Cyclic voltammograms obtained in deoxygenated 0.1 M $HClO_4$ solution after every 5000 cycles for Pt~$Pd_{0.90}Ni_{0.10}$ core−shell composites. In the inset, the measured ESA loss is also shown as a function of durability cycling for the Pt~$Pd_{0.90}Ni_{0.10}$ architecture. (B) The corresponding polarization curves, obtained in an oxygen saturated 0.1 M $HClO_4$ at 1600 rpm after every 5000 cycles. Area-specific activities, measured at 0.9 V, are plotted as a function of durability in the inset.

enhanced activity to the preferential dissolution of both Pd and Ni content in the core as well as to a restructuring of the Pt monolayer. Overall, our results demonstrate that our Pt~$Pd_{0.90}Ni_{0.10}$ electrocatalysts possess excellent electrochemical stability.

4. CONCLUSIONS

In this report, we have utilized an ambient, surfactant-based synthetic method to prepare ultrathin, composition-tunable, Pd−Ni one-dimensional nanostructures possessing high structural uniformity and a homogeneous distribution of elements. The electrochemical activities of the carbon-supported Pd−Ni were examined. Two of the compositions, namely, $Pd_{0.90}Ni_{0.10}$ and $Pd_{0.83}Ni_{0.17}$, exhibited either similar or higher specific activities by comparison with elemental Pd NWs, whereas all four chemical compositions of the nanowires tested, which were involved in electrochemical tests (namely elemental Pd, $Pd_{0.90}Ni_{0.10}$, $Pd_{0.83}Ni_{0.17}$, and $Pd_{0.75}Ni_{0.25}$) possessed measurable enhancement as compared with

dx.doi.org/10.1021/cs500125y | ACS Catal. 2014, 4, 2544−2555

commercial Pd nanoparticles. More importantly, as a positive indicator of the potential practicality of our research herein, the $Pd_{0.90}Ni_{0.10}$ sample exhibited outstanding methanol tolerance ability. In essence, there was only a 15% loss in the specific activity in the presence of 4 mM of methanol.

Moving beyond the "bimetallic" structural motif, we also studied ultrathin, core−shell Pt∼$Pd_{0.90}Ni_{0.10}$ nanowires, which exhibited a specific activity of 0.62 mA/cm^2 and a corresponding mass activity of 1.44 A/mg$_{Pt}$. Moreover, our as-prepared core−shell catalyst maintained excellent electrochemical durability under realistic testing conditions, with the specific activity of our as-prepared electrocatalysts actually increasing by more than 20% after 10 000 cycles from 0.62 to 0.76 mA/cm^2. We attributed the improvement in both catalytic performance and stability not only to the surface contraction of the Pt layer due to the small dimensions of the wires but also to the electronic effect that the nanoscale Pd−Ni alloy core imparts to the outer Pt monolayer shell. Further investigation in terms of determining the detailed electronic structure of ultrathin Pt∼Pd−Ni nanowires may lead to a better understanding of the role of chemical composition in determining overall electrocatalytic behavior. Nonetheless, we postulate that 1-D Pd−Ni nanostructures represent a promising platform for designing ORR catalysts with respectable activity. In so doing, we are able to offer these nanowires as a more earth-abundant, lower cost, high-performance, and, therefore, attractive alternative to the conventional use of Pt nanoparticles as ORR catalysts.

■ ASSOCIATED CONTENT

Supporting Information

Additional structural and electrochemical characterization data of the nanowires. This material is available free of charge via the Internet at http://pubs.acs.org.

■ AUTHOR INFORMATION

Corresponding Author

*E-mail: stanislaus.wong@stonybrook.edu; sswong@bnl.gov.

Notes

The authors declare no competing financial interest.

■ ACKNOWLEDGMENTS

Research (including funding for H.L., C.K., and S.S.W., and electrochemical experiments) was supported by the U.S. Department of Energy, Basic Energy Sciences, Materials Sciences and Engineering Division. We also would like to thank M. B. Vukmirovic for technical assistance with electrochemical measurements at Brookhaven National Laboratory, which is supported by the U.S. Department of Energy under Contract No. DE-AC02-98CH10886.

■ REFERENCES

(1) Shukla, A. K.; Ravikumar, M. K.; Gandhi, K. S. *J. Solid State Electrochem.* **1998**, *2* (2), 117−122.
(2) Aricò, A. S.; Srinivasan, S.; Antonucci, V. *Fuel Cells* **2001**, *1* (2), 133−161.
(3) Chen, C. Y.; Liu, D. H.; Huang, C. L.; Chang, C. L. *J. Power Sources* **2007**, *167* (2), 442−449.
(4) Renock, D. L., Hanwei; Zhang, P.; Ma, J.; Peiter, C.; Samuel, S.; Litt, M. In *Direct Methanol Fuel Cells for Portable Electronics*, 41st Power Sources Conference, 2004; National Technical Information Service: Alexandria, VA, 2004.
(5) Lamy, C.; Belgsir, E. M.; Leger, J. M. *J. Appl. Electrochem.* **2001**, *31* (7), 799−809.
(6) Peled, E.; Duvdevani, T.; Aharon, A.; Melman, A. *Electrochem. Solid-State Lett.* **2001**, *4* (4), A38−A41.
(7) Litster, S.; McLean, G. *J. Power Sources* **2004**, *130* (1−2), 61−76.
(8) Antolini, E. *J. Appl. Electrochem.* **2004**, *34* (6), 563−576.
(9) Koenigsmann, C.; Wong, S. S. *Energy Environ. Sci.* **2011**, *4* (4), 1161−1176.
(10) Koenigsmann, C.; Scofield, M. E.; Liu, H.; Wong, S. S. *J. Phys. Chem. Lett.* **2012**, *3* (22), 3385−3398.
(11) Savadogo, O.; Lee, K.; Oishi, K.; Mitsushima, S.; Kamiya, N.; Ota, K. I. *Electrochem. Commun.* **2004**, *6* (2), 105−109.
(12) Savadogo, O.; Lee, K.; Mitsushima, S.; Kamiya, N.; Ota, K. I. *J. New Mater. Electrochem. Syst.* **2004**, *7* (2), 77−83.
(13) Løvvik, O. M. *Surf. Sci.* **2005**, *583* (1), 100−106.
(14) Greeley, J.; Norskov, J. K. *Surf. Sci.* **2005**, *592* (1−3), 104−111.
(15) Li, B.; Prakash, J. *Electrochem. Commun.* **2009**, *11* (6), 1162−1165.
(16) Li, B.; Amiruddin, S.; Prakash, J. *ECS Trans.* **2008**, *6* (25), 139−144.
(17) Zhao, J.; Sarkar, A.; Manthiram, A. *Electrochim. Acta* **2010**, *55* (5), 1756−1765.
(18) Liu, L.; Samjeske, G.; Nagamatsu, S.-i.; Sekizawa, O.; Nagasawa, K.; Takao, S.; Imaizumi, Y.; Yamamoto, T.; Uruga, T.; Iwasawa, Y. *Top. Catal.* **2013**, 1−12.
(19) Ramos-Sanchez, G.; Bruno, M. M.; Thomas, Y. R. J.; Corti, H. R.; Solorza-Feria, O. *Int. J. Hydrogen Energy* **2012**, *37* (1), 31−40.
(20) Ramos-Sanchez, G.; Yee-Madeira, H.; Solorza-Feria, O. *Int. J. Hydrogen Energy* **2008**, *33* (13), 3596−3600.
(21) Wang, R. F.; Li, H.; Ji, S.; Wang, H.; Lei, Z. Q. *Electrochim. Acta* **2010**, *55* (5), 1519−1522.
(22) Shao, M. H.; Smith, B. H.; Guerrero, S.; Protsailo, L.; Su, D.; Kaneko, K.; Odell, J. H.; Humbert, M. P.; Sasaki, K.; Marzullo, J.; Darling, R. M. *Phys. Chem. Chem. Phys.* **2013**, *15* (36), 15078−15090.
(23) Tarasevich, M. R.; Zhutaeva, G. V.; Bogdanovskaya, V. A.; Radina, M. V.; Ehrenburg, M. R.; Chalykh, A. E. *Electrochim. Acta* **2007**, *52* (15), 5108−5118.
(24) Weber, J.; Singhal, R.; Zekri, S.; Kumar, A. *Int. Mater. Rev.* **2008**, *53* (4), 235−255.
(25) Wang, N.; Cai, Y.; Zhang, R. Q. *Mater. Sci. Eng., R* **2008**, *60* (1−6), 1−51.
(26) Cademartiri, L.; Ozin, G. A. *Adv. Mater.* **2009**, *21* (9), 1013−1020.
(27) Xia, Y. N.; Yang, P. D.; Sun, Y. G.; Wu, Y. Y.; Mayers, B.; Gates, B.; Yin, Y. D.; Kim, F.; Yan, Y. Q. *Adv. Mater.* **2003**, *15* (5), 353−389.
(28) Lim, B.; Jiang, M. J.; Camargo, P. H. C.; Cho, E. C.; Tao, J.; Lu, X. M.; Zhu, Y. M.; Xia, Y. N. *Science* **2009**, *324* (5932), 1302−1305.
(29) Koenigsmann, C.; Sutter, E.; Chiesa, T. A.; Adzic, R. R.; Wong, S. S. *Nano Lett.* **2012**, *12* (4), 2013−2020.
(30) Koenigsmann, C.; Sutter, E.; Adzic, R. R.; Wong, S. S. *J. Phys. Chem. C* **2012**, *116* (29), 15297−15306.
(31) Teng, X. W.; Han, W. Q.; Ku, W.; Hucker, M. *Angew. Chem. Int. Ed.* **2008**, *47* (11), 2055−2058.
(32) Koenigsmann, C.; Santulli, A. C.; Gong, K. P.; Vukmirovic, M. B.; Zhou, W. P.; Sutter, E.; Wong, S. S.; Adzic, R. R. *J. Am. Chem. Soc.* **2011**, *133* (25), 9783−9795.
(33) Sasaki, K.; Naohara, H.; Choi, Y. M.; Cai, Y.; Chen, W. F.; Liu, P.; Adzic, R. R. *Nat. Commun.* **2012**, 3.
(34) Wang, J. X.; Inada, H.; Wu, L.; Zhu, Y.; Choi, Y.; Liu, P.; Zhou, W.-P.; Adzic, R. R. *J. Am. Chem. Soc.* **2009**, *131* (47), 17298−17302.
(35) Garsany, Y.; Baturina, O. A.; Swider-Lyons, K. E.; Kocha, S. S. *Anal. Chem.* **2010**, *82* (15), 6321−6328.
(36) Stamenkovic, V. R.; Fowler, B.; Mun, B. S.; Wang, G.; Ross, P. N.; Lucas, C. A.; Marković, N. M. *Science* **2007**, *315* (5811), 493−497.
(37) Bandarenka, A. S.; Varela, A. S.; Karamad, M.; Calle-Vallejo, F.; Bech, L.; Perez-Alonso, F. J.; Rossmeisl, J.; Stephens, I. E. L.; Chorkendorff, I. *Angew. Chem., Int. Ed.* **2012**, *51* (47), 11845−11848.

(38) *The US DRIVE Fuel Cell Technical Team Technology Roadmap*; revised June 2013; http://energy.gov/sites/prod/files/2014/02/f8/fctt_roadmap_june2013.pdf; accessible June 2014.
(39) Alia, S. M.; Larsen, B. A.; Pylypenko, S.; Cullen, D. A.; Diercks, D. R.; Neyerlin, K. C.; Kocha, S. S.; Pivovar, B. S. *ACS Catal.* **2014**, *4* (4), 1114−1119.
(40) *Calculated Ni-Pd Phase Diagram*. National Physical Laboratory of the United Kingdom: Teddington, Middlesex, U.K.; http://resource.npl.co.uk/mtdata/phdiagrams/nipd.htm, 2000.
(41) Lee, K.; Savadogo, O.; Ishihara, A.; Mitsushima, S.; Kamiya, N.; Ota, K.-i. *J. Electrochem. Soc.* **2006**, *153* (1), A20.
(42) Wu, J.; Zhang, J.; Peng, Z.; Yang, S.; Wagner, F. T.; Yang, H. *J. Am. Chem. Soc.* **2010**, *132* (14), 4984−4985.
(43) Adzic, R. R.; Zhang, J.; Sasaki, K.; Vukmirovic, M. B.; Shao, M.; Wang, J. X.; Nilekar, A. U.; Mavrikakis, M.; Valerio, J. A.; Uribe, F. *Top. Catal.* **2007**, *46* (3−4), 249−262.
(44) Ham, D. J.; Pak, C.; Bae, G. H.; Han, S.; Kwon, K.; Jin, S. A.; Chang, H.; Choi, S. H.; Lee, J. S. *Chem. Commun. (Cambridge)* **2011**, *47* (20), 5792−5794.
(45) Bozzolo, G.; Noebe, R. D.; Khalil, J.; Morse, J. *Appl. Surf. Sci.* **2003**, *219* (1−2), 149−157.
(46) Koenigsmann, C.; Zhou, W. P.; Adzic, R. R.; Sutter, E.; Wong, S. S. *Nano Lett.* **2010**, *10* (8), 2806−2811.
(47) Zhang, J.; Vukmirovic, M. B.; Sasaki, K.; Nilekar, A. U.; Mavrikakis, M.; Adzic, R. R. *J. Am. Chem. Soc.* **2005**, *127*, 12480−12481.
(48) Lima, F. H. B.; Lizcano-Valbuena, W. H.; Texeira-Neto, E.; Nart, F. C.; Gonzalez, E. R.; Ticianelli, E. A. *Electrochim. Acta* **2006**, *52*, 385−393.
(49) Hsu, S.-P.; Liu, C.-W.; Chen, H.-S.; Chen, T.-Y.; Lai, C.-M.; Lee, C.-H.; Lee, J.-F.; Chan, T.-S.; Tsai, L.-D.; Wang, K.-W. *Electrochim. Acta* **2013**, *105*, 180−187.
(50) Xing, Y.; Cai, Y.; Vukmirovic, M. B.; Zhou, W.-P.; Karan, H.; Wang, J. X.; Adzic, R. R. *J. Phys. Chem. Lett.* **2010**, *1* (21), 3238−3242.
(51) Sasaki, K.; Naohara, H.; Cai, Y.; Choi, Y. M.; Liu, P.; Vukmirovic, M. B.; Wang, J. X.; Adzic, R. R. *Angew. Chem., Int. Ed.* **2010**, *49* (46), 8602−8607.